

---

# Beta Camera for Static and Dynamic Imaging of Charged-Particle Emitting Radionuclides in Biologic Samples

Kaj Ljunggren and Sven-Erik Strand

*Radiation Physics Department, Lund University, Lund, Sweden*

---

A detection system based on microchannel plates has been constructed to image charged particles emitted by radionuclides in biomedical samples. This technique has significant advantages over conventional film autoradiography for investigating the distribution of radiolabeled compounds: shorter acquisition times due to the high sensitivity, easier sample handling, direct quantification and the ability to perform dynamic studies. The detector performance shows a spatial resolution of 0.9 mm for carbon-14 ( $^{14}\text{C}$ ) (0.156 MeV), good linearity and homogeneity. The noise level is below 50/( $\text{cm}^2 \cdot \text{sec}$ ). Successful imaging with this system has been performed with beta-emitters  $^{14}\text{C}$ , sulfur-35 ( $^{35}\text{S}$ ), iodine-131 ( $^{131}\text{I}$ ), yttrium-90 ( $^{90}\text{Y}$ ), and positron emitters gallium-68 ( $^{68}\text{Ga}$ ), and fluorine-18 ( $^{18}\text{F}$ ). Dynamic studies of axonal transport of  $^{35}\text{S}$ -methionine in a nerve, and static images of  $^{90}\text{Y}$ -labeled monoclonal antibodies in slices of tumors are presented. The system shows promise for rapid quantitative imaging of charged-particle emitting radionuclides in small biologic samples.

**J Nucl Med 1990; 31:2058-2063**

---

Labeled monoclonal antibodies have been increasingly used for cancer therapy and diagnostics. Consequently, calculation of absorbed dose to tumor tissue and normal organs has become an important problem. It is now recognized that the distribution of antibodies in the tumor tissue is not uniform as has been assumed in conventional absorbed dose calculations (1-3). Therefore, detailed information about the distribution of radioactive substances is necessary for an accurate absorbed dose calculation in tumor tissue. This essential information can be obtained through autoradiography (2,3). However, this procedure is time consuming and requires extremely long exposure times. Furthermore, the film characteristic is not linear and has a relatively narrow dynamic range (4). Quantitative data from autoradiographs can be obtained with a densitometer or

via image processing with a video camera (5-7). Dynamic studies with charged-particle emitters are usually performed by cutting consecutive slices of sacrificed animals and by measurements in liquid scintillation detectors (8).

To overcome the aforementioned difficulties, a new detection system that is capable of imaging charged particles emitted by radionuclides distributed in tissue slices has been developed. This "beta camera" uses a plastic scintillator plus a photon-counting detector containing a photo-cathode, microchannel plates (MCP), and a resistive anode. Microchannel-plates have been used for 20 yr as position detectors in physics for electrons, ions, X-rays, soft X-rays and ultra-violet (UV) (9). Since 1979, a variety of two-dimensional photon counting techniques have been developed, using MCP and several types of position sensitive anodes (10-12). Microchannel plate detectors have recently been utilized extensively for detection of low intensity UV-light in astronomical applications, such as spaceborn imaging and spectroscopy (13).

## MATERIALS AND METHODS

### Detector Design

The detection system consists primarily of a plastic scintillator and a light sensitive detector. The main characteristics are given in Table 1.

The charged particle detector is a plastic scintillator of 0.9 mm thickness and a diameter of 40 mm (NE 102A, Nuclear Enterprises Ltd., Beenham Reading, England). It is mounted directly in contact with the fiber-optic window on the light sensitive detector with an optical gel (OC-2 0057, Dow Corning Corp., Midland, Michigan).

The light photon-sensitive detector consists of a fiber-optic window, a photo-cathode, two MCPs and a resistive anode. The photo-cathode (S20 multi-alkali) is evaporated on the inside of the fiber optic window (Fig. 1). The front MCP is coated with a thin, 5nm, aluminum oxide film to prevent ion feedback within the MCP from bombarding the photo-cathode, with a consequent reduction of its useful lifetime. The diameter of the fiber-optic window is 40 mm. The whole detector assembly is placed in a high-vacuum tube fabricated by ITL Ltd., St. Leonards on Sea, UK to our specifications.

---

Received Nov. 14, 1988; revision accepted June 11, 1990.  
For reprints contact: Kaj Ljunggren, BSc, Radiation Physics Dept., Lund Univ., Lasarettet, S-22185, Lund, Sweden.

**TABLE 1**  
Main Characteristics of the Detector System

Window material	Glass fiber optic
Window thickness	15 mm
Fiber-optic channel diameter	8 $\mu\text{m}$
Field of view	diameter 40 mm
Central field of view	diameter 30 mm
Photo-cathode	S 20
Proximity focusing gap	750 $\mu\text{m}$
MCP-type	Chevron, V-type
MCP channel diameter	12 $\mu\text{m}$
Ion barrier	5 nm, aluminum oxide
MCP-anode gap	5.0 mm
Anode design	Resistive, CAT
Scintillator	Plastic NE 102A 0.9 mm

All the internal components are powered by a voltage divider through a high voltage unit. The detector is operated at a high voltage of 3.4 kV for beta particles and 3.1 kV for alpha particles. The preset energy window requires that the operating voltage for alpha-particle- and beta-particle-counting be slightly different. The resistive anode is connected from each corner to four amplifiers. Each amplifier consists of a charge sensitive preamplifier and a pulse-shaping unit (linear amplifier). A position analyzer handles the signals from the amplifiers and generates analog x- and y-signals and a digital strobe. These signal lines are connected to an ADC, an acquisition unit, and an image processing system (Fig. 2).

### Detector Principle

An interaction of a charged particle in the plastic scintillator produces light photons. These light photons are then transferred through the fiber-optic window to the photo-cathode, where photoelectrons are generated. The MCP consists of  $5 \times 10^5$  channels/cm<sup>2</sup> (diameter 12  $\mu\text{m}$ ) each working as a conventional PM-tube, but with a continuous dynode system. The inner side of the microchannels is coated with a semiconducting layer, with a high secondary electron emission coefficient (11,12). Due to the potential difference of 400 V maintained between cathode and MCP, the electrons are accelerated and gain enough energy to knock out further electrons. An electron cascade is therefore generated in the MCP, with a gain of about  $10^6$  to  $10^7$ .

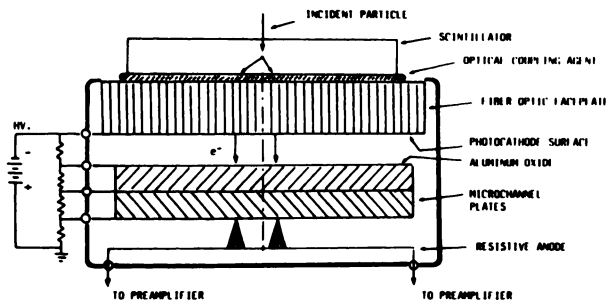


**FIGURE 1**  
The 'beta camera.' Schematic drawing of the detection system. Note that the channels are configured in an angle. Because of this mounting of the two channel plates, the detector is configured in so-called V-stack- or Chevron-configuration.

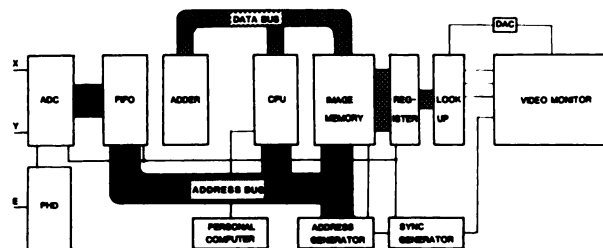


**FIGURE 2**  
Block diagram of the components in the image memory. Position signals (x, y) are fed into an ADC together with the energy signal through a pulse-height discriminator. (FIFO = first in first out memory, CPU = central processor unit and DAC = digital-analog converter). The image memory is updated in real time event for event.

When the electron cascade strikes the square resistive anode, pulses are generated with amplitudes depending on its position. This procedure is similar to that in scintillation cameras, whereby positional information is obtained from events interacting in the NaI(Tl) crystal. The algorithm to obtain x- and y-coordinates of an event is as follows:

$$X = \frac{Q_A + Q_B - (Q_C + Q_D)}{Q_A + Q_B + Q_C + Q_D}$$

and

$$Y = \frac{Q_A + Q_D - (Q_B + Q_C)}{Q_A + Q_B + Q_C + Q_D}$$

where  $Q_A$  (upper left corner),  $Q_B$  (upper right corner),  $Q_C$  (lower left corner), and  $Q_D$  (lower right corner) represent the charge signals at each of the anode's four terminals. An energy signal is obtained by summing all pulses from the position coordinates, which are then fed to a pulse-height discriminator (PHD) (Fig. 2).

The detection system is kept in a freezer operating at  $-20^\circ\text{C}$  to cool the photo-cathode, thereby keeping the noise level as low as possible. It is also necessary to keep the detector system shielded from light, in that the plastic scintillator is not sealed with any material that can prevent external light photons from falling on the detector. If exposed to light, it will take 24 hr before the noise level is stabilized again.

### Image Memory and Image Processor

A dedicated image memory unit, based on an 8-bit 8085 microprocessor (INTEL Corp., Santa Clara, CA) is connected to a host computer as shown in Figure 2. The image matrix consists of  $128 \times 128$  pixels. An external TV-monitor connected to the image memory can display the matrix (in real time) in 256 gray levels (video signal) or 8 colors (RGB-signal). Normalization and discrimination of the image is performed by a look-up table, which decodes data without changing raw data. The detector signals are digitized and define the x-y-addresses in the image memory. The acquisition unit is directly connected to the memory, guaranteeing a fast acquisition rate. A software package, written in ANSI 66 Standard Fortran for a host computer, performs manipulations and calculations on the image. Several options for image processing have been added. The computer also stores images on files for floppy discs.

## MEASUREMENTS OF DETECTOR PERFORMANCE

### Linearity

A point source matrix consisting of  $^{14}\text{C}$  filled holes in an experimental print card with a quadratic spacing of 8 mm between the holes, was placed in contact with the detector, and imaging was performed. Measurements of the detector linearity were performed according to the NEMA protocol (14) by determination of the maximum displacement of peak locations in the image from the holes of the point sources (x,y).

### Homogeneity

An absorbing paper, cut to the dimensions of the detector was immersed in  $^{14}\text{C}$ -solution, and then allowed to dry. The plane source was covered with mylar foil (3  $\mu\text{m}$ ) (Du Pont, Stockholm, Sweden) and mounted onto a plastic sheet as a carrier. This assembly was then positioned on the detector and imaged. Homogeneity measurements were performed by registering the maximum deviation in the image for a matrix size of 128  $\times$  128 over central field of view (CFOV) (14)

### Energy Resolution

To test the energy resolution capabilities of the detector system, two radioisotopes, gallium-67 ( $^{67}\text{Ga}$ ) and indium-113m ( $^{113\text{m}}\text{In}$ ) that emit monoenergetic conversion electrons were selected. Conversion electrons of 83 keV energy with an abundance of 0.28 are emitted by  $^{67}\text{Ga}$ , whereas 360 keV electrons are emitted by  $^{113\text{m}}\text{In}$  with a yield of 0.27 (15). Small aliquots of these isotopes were placed on a plastic sheet, which was then covered with a 3- $\mu\text{m}$  mylar foil. Pulse-height distributions were recorded with a pulse-height analyzer (ND 62 Nuclear Data Inc., Schaumburg, IL).

### Spatial Resolution

Line sources were prepared by immersing a sewing thread of 0.5 mm diameter in  $^{14}\text{C}$ -solution and allowing it to dry. Approximately 4 cm long line sources were prepared and glued onto a 0.5-mm thick plastic sheet and covered with a 3- $\mu\text{m}$  mylar foil to prevent contamination of the scintillator. The line sources were placed in contact with the detector for imaging. The acquisition was performed in zoom mode. The spatial resolution, determined as full width at half maximum (FWHM) (14) was measured.

## RESULTS

### Detector Performance

**Linearity.** Figure 3A shows the image of the point source matrix consisting of the  $^{14}\text{C}$  activity dots. The

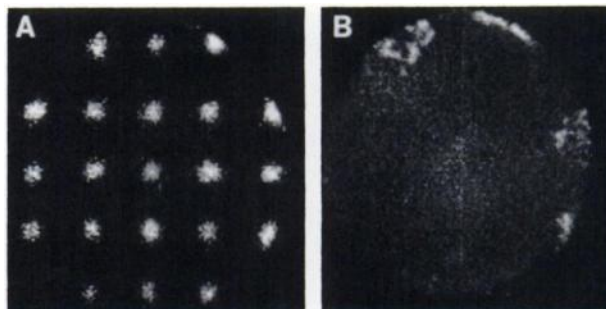


**FIGURE 3**  
(A) The image of the point source matrix showing good linearity of the system. (B) Homogeneity of 'beta camera.'

result shows an absolute linearity of 0.4 mm in the CFOV. The varying intensity of the dots in this figure is due to differences in the activity content.

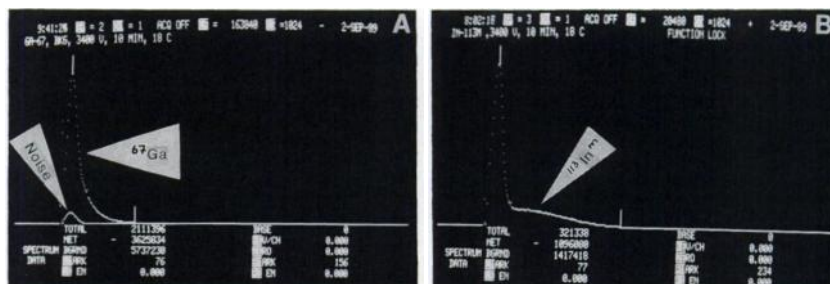
**Homogeneity.** The image of the homogeneous  $^{14}\text{C}$  phantom is shown in Figure 3B. The integral homogeneity is 35% over the CFOV. Outside this area we have hot spots corresponding to the discharges at the points where the MCP have been mounted.

**Energy Resolution.** Figures 4A and 4B show two pulse-height distributions for conversion electrons from  $^{67}\text{Ga}$  and  $^{113\text{m}}\text{In}$ . Because of the low electron energy for  $^{67}\text{Ga}$  (83 keV), the pulse-height distribution is just detectable above the noise distribution as seen in Figure 4A. The higher electron energy for  $^{113\text{m}}\text{In}$  (360 keV), however, is clearly distinguishable from the noise and the pulse-height distribution shows a peak distribution with a large spread, indicative of an inadequate energy resolution. Figures 4A and 4B show the shape of the spectrum for different energies. The left marker shows the peak for single events (including noise) and the right shows the energy for multiple events. Whereas the noise only gives single events, multiple events are the ones useful for imaging.

**Spatial Resolution.** The spatial resolution measured as FWHM of the  $^{14}\text{C}$  line source was 0.9 mm. The line spread function is shown in Figure 5.

**Noise.** The thermal noise was measured to be 50/( $\text{cm}^2 \text{ sec}$ ) (CFOV) at room temperature, and was a factor 5 lower at  $-20^\circ\text{C}$ .

**FIGURE 4**  
Pulse height distributions from conversion electron emitters (A)  $^{67}\text{Ga}$  and (B)  $^{113\text{m}}\text{In}$  with a high voltage setting of 3.4 kV.



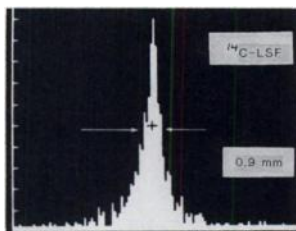


**FIGURE 5.**  
Spatial resolution measured as FWHM of  $^{14}\text{C}$  line source.

## APPLICATIONS WITH IMAGING OF BIOLOGIC SAMPLES

### Comparison of Autoradiography and Beta Camera

A biologic sample consisting of a 20- $\mu\text{m}$  thick whole-body slice of a mouse injected with  $^{14}\text{C}$ -SAS9244 (12 kBq/g body weight) was obtained from the Dept. of Toxicology, Uppsala, Sweden. A circular part of the whole-body slice (diameter 40 mm) was cut out for beta camera imaging during 6 hr.

The same sample was also autoradiographed using conventional film technique over a period of 52 days. The results are given in Figures 6A-B. It can be seen that the beta camera is capable of providing a detailed image much faster than conventional autoradiography, while maintaining reasonably good spatial resolution. The ability to obtain direct quantitative information is an additional advantage of the beta camera.

### Static Images

**Monoclonal Antibodies in Tumors.** Nude rats were heterotransplanted with human melanoma tumors. One week after the injection of  $^{131}\text{I}$ -labeled 96.5 monoclonal antibodies (16), the animals were killed, the tumors were taken out, and 40- $\mu\text{m}$  thick frozen sections of the tumors were obtained. The sections were then mounted on a thin plastic sheet and covered with a 3- $\mu\text{m}$  thick mylar foil. The absorption in the mylar foil of the energetic beta-particles ( $E_{\text{max}} = 0.606 \text{ MeV}$ ) emitted by  $^{131}\text{I}$  is negligible. The sample was placed on the beta camera for imaging. Figure 7 shows the activity distribution of  $^{131}\text{I}$  in the tumor tissue. It is clear that the distribution is nonuniform in the tumor, with several areas of high concentration of radioactivity.

Since  $^{90}\text{Y}$ -labeled antibodies are increasingly used for treatment, the ability to image the energetic beta-particles ( $E_{\text{max}} = 2.27 \text{ MeV}$ ) emitted by this radionuclide was tested. Nude mice bearing xenografted human ser-

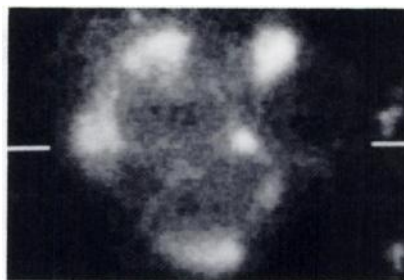


**FIGURE 7**  
Beta camera image of a slice of a human melanoma tumor grown in a nude rat, showing the activity distribution of  $^{131}\text{I}$ -96.5 monoclonal antibodies. Acquisition time 6 hr.

ous ovarian cancer were injected with  $^{90}\text{Y}$ -labeled monoclonal antibodies reacting against fibrin (59D8 Fab fragment, provided by K. Kairemo, Helsinki, Finland) (17). Tumor tissue was taken out and prepared for imaging on the beta camera as described above. In Figure 8A, the histologic sections containing tumor tissue are shown, and in Figure 8B the corresponding  $^{90}\text{Y}$  activity distribution within these sections are given.

### Dynamic Studies

A sciatic nerve from a frog (*R. temporana*) with its attached dorsal root ganglia (DRG) was removed by dissection. A ligature was applied on the nerve. The DRGs were each injected with 2  $\mu\text{l}$  Ringer solution supplemented with  $^{35}\text{S}$ -methionine (0.2-0.4 MBq/ganglia). The nerve was then mounted in an incubation chamber covered with mylar foil, and the chamber was mounted on the detector face plate. Images were recorded every second hour for 24 hr with 15 min acquisition time. Figures 9A-D correspond to 0, 8, 16, and 24 hr postinjection. The time-activity curve for the uptake in one part of the axon is given in Figure 9E. This illustrates the usefulness of our system for dynamic studies. All results obtained above are very similar to conventional scintillation camera imaging, here however for beta-emitting radionuclides.

## DISCUSSION

Our beta camera has been shown to be capable of imaging charged-particle emitting radionuclides in biologic samples with short acquisition times. Both static

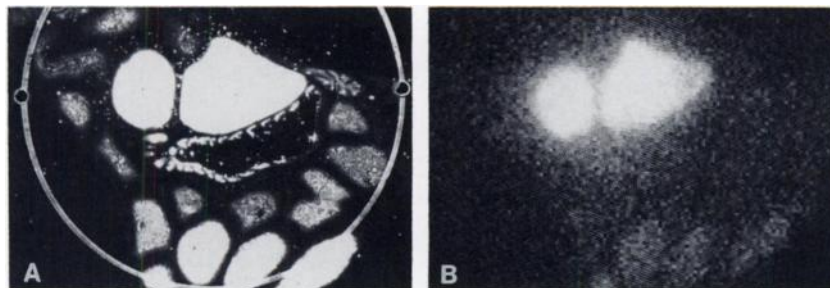
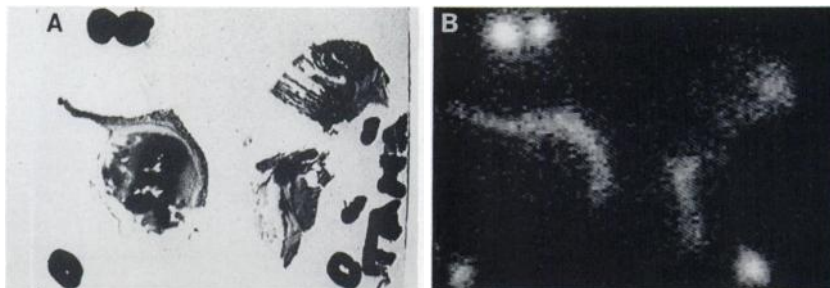


**FIGURE 6**  
(A) Conventional autoradiography of  $^{14}\text{C}$  activity in a 20- $\mu\text{m}$  thick slice of a rat. Exposure time 52 days. (B) Same slice obtained during 6 hr with the 'beta camera.'

**FIGURE 8**

Human ovarian tumors grown in nude mice injected with  $^{90}\text{Y}$  Fab fragments. (A) Histologic slices. (B) Beta camera image with exposure time 10 min.



and dynamic images can be performed. The detector performance shows good linearity. The uniformity constant however was not as good in our first detector, can be corrected in the same way as scintillation cameras. There are good possibilities for energy discrimination in the system. Further improvements of the detector are possible. The spatial resolution, which is currently 0.9 mm FWHM, can be improved, for example, by minimizing the amount of optical light reflected within the scintillator.

By painting the scintillator black except on the side against the fiber optic window, Schrack et al. (18) improved the spatial resolution for a similar detector for neutron measurements from 0.93 mm to 0.51 mm. Another method of improvement is the use of a thinner scintillator. Also, optimization of the voltage settings of the individual plates in the detector can improve the spatial resolution (Clampin, *personal communication*, 1990).

The current beta camera detector consists of a V-stack MCP configuration (Chevron). Microchannel plates in the form of V-Z-stack (Ranicon-detector) give a gain of the order of  $10^8$  or higher (19). Removal of the aluminum oxide-film has also shown to improve the spatial resolution (20). Replacing the resistive anode with, for example, a wedge and strip anode, may further

improve the spatial resolution. In a 1988 investigation, Clampin et al. (20) showed that an optical resolution (without scintillator) of a Ranicon detector of 30–50  $\mu\text{m}$  is achievable.

Our second generation system has recently been constructed, including some of the above suggestions based on a Z-stacked MCP, and is supposed to give a spatial resolution in the order of 0.5 mm.

Our image memory today consists of only an 8-bit microprocessor. An upgrading of the image memory is underway, using a 16-bit 68000 Motorola microprocessor connected to a 32-bit 80386 minicomputer. The new image memory consists of  $256 \times 256$  pixels with 16-bit depths giving 4096 color levels. This improvement will give images with better resolution and statistics.

Investigations of biologic tissue samples and dynamic studies of retrograde axonal transport clearly show that the beta camera is quite capable of imaging the tissue distribution of radioactivity, as well as providing quantitative data. In one other experiment (not shown) we imaged simultaneously  $^{18}\text{F}$ FDG and  $^{35}\text{S}$ -intrinsically labeled monoclonal antibodies (21) in tumors, utilizing the short half-life of  $^{18}\text{F}$ . Both metabolic and uptake measurements could easily be performed within a one day exposure time.

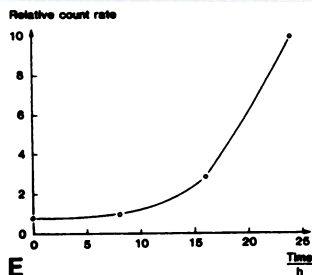
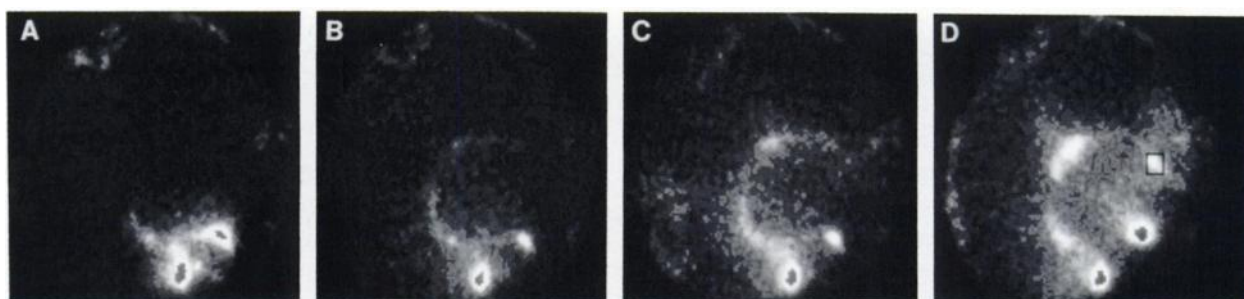


**FIGURE 9**

Dynamic study with the beta camera of the axonal transport of  $^{35}\text{S}$ -methionine injected in the ganglion of a frog nerve. Images at (A) 0 hr, (B) 8 hr, (C) 16 hr, and (D) 24 hr after the injection. (E) The time activity curve generated from the square ROI shown in (D).

In addition to these studies, alpha-emitters have also been imaged. As an example, a sample containing curium-244, which emits 5.8 MeV alpha-particles, was successfully imaged by the beta camera (unpublished data).

## CONCLUSION

We have constructed a beta camera with which we have been able to detect charged-particle emitting radionuclides in biologic samples. This instrument has valuable properties: high sensitivity and ability to process individual events with a computer and display system. With this system it is possible to make very rapid acquisitions compared to conventional film-autoradiographic techniques as well as to perform dynamic studies on living samples, i.e., nerve tissues in nutrient solution. We believe that this detector system can replace the film technique to some extent and make quantitative studies much easier.

The system is very useful for rapid acquisition of radionuclide distribution data from biologic samples and may be invaluable in biomedical research. Further work to improve the detector characteristics is underway.

## ACKNOWLEDGMENTS

The authors thank the Swedish Natural Science Research Council (grant no. F-FU 1621-111), Swedish Association for Technical Support (grant no. 89-02474P), John and Augusta Persson's Foundation for Scientific Medical Research, B. Kamprads Foundation for Cancer Research, Lund, and the Faculty of Medicine for financial support of this work.

We also thank Bengt Larsson, Martin Kanje, and Agneta Persson, for helping us with the biologic samples and K. Kairemo for supplying us with tumor sections. We also thank Professor D. Rao for comments during the preparation of this manuscript.

## REFERENCES

1. Ingvar C, Jacobsson B, Brodin T, Jönsson P-E, Strand S-E. Tumour antigen heterogeneity within melanoma metastases. An evaluation by immunohistochemistry. *Anticancer Res* 1990; in press.
2. Del Vecchio S, Reynolds JC, Blasberg RG, et al. Measurement of local M<sub>1</sub>97,000 and 250,000 protein antigen concentration in sections of human melanoma tumor using in vitro quantitative autoradiography. *Cancer Res* 1988; 48:5475-5481.
3. Ingvar C, Norrgren K, Strand S-E, Jönsson P-E. Heterogeneous distribution of radiolabelled monoclonal antibody. Autoradiographic evaluation in the nude rat model. *Anticancer Res*.
4. Ullberg S, Larsson B, Tjävle H. Autoradiography. In: Glenn HJ, Colombetti LG, eds. *Biologic applications of radiotracers*. Boca Raton, FL: CRC Press, Inc.; 1982 55-108.
5. Yonekura Y, Brill AB, Som P, Bennet GW, Fand I. Quantitative autoradiography with radiopharmaceuticals, part 1: digital film-analysis system by videodensitometry: concise communication. *J Nucl Med* 1983; 24:231-237.
6. Som P, Yonekura Y, Oster ZH, et al. Quantitative autoradiography with radiopharmaceuticals, part 2: applications in radiopharmaceutical research. concise communication. *J Nucl Med* 1983; 24:238-244.
7. d'Argy R. Short-lived radionuclides and image analysis in whole-body autoradiography. [Thesis] *Acta Univ Upsaliensis* 1988; 40:1-47.
8. Edstöm A, Mattson H. Fast axonal transport in vitro in the sciatic system of the frog. *J Neurochem* 1972; 19:205-221.
9. Wiza JL. Microchannel plate detectors. *Nucl Instrum Methods* 1979; 162:587-601.
10. Lampton M, Carlson CW. Low-distortion resistive anodes for two-dimensional position-sensitive MCP systems. *Rev Sci Instrum* 1979; 50:1093-1097.
11. Rees D, MacWhirter I, Rounce PA, Barlow FE, Kellock SJ. Minature imaging photon detectors. *J Phys [E]* 1980; 13:763-770.
12. Rees D, MacWhirter I, Rounce PA, Barlow FE. Minature imaging photon detectors II. *J Phys [E]* 1981; 14:229-233.
13. Clampin M, Edwin RP. Large format imaging photon detector for astronomical spectroscopy. *Rev Sci Instrum* 1987; 58:167-172.
14. Performance Measurements of Scintillation Cameras, NEMA Standards Publication NU 1-1986.
15. Browne E, Firestone RB. In: Shirley V, ed. *1986 table of radioactive isotopes*. New York: John Wiley & Sons; 1986.
16. Ingvar C, Norrgren K, Strand S-E, Brodin T, Jönsson P-E, Sjögren H-O. Biokinetics of radiolabeled monoclonal antibodies in heterotransplanted nude rats: evaluation of corrected specific tissue uptake. *J Nucl Med* 1989; 30:1224-1234.
17. Kairemo K, Ljunggren K, Strand S-E, Wahlström T, Penttilä PI, Hiltunen JV. The follow-up of radioimmunotherapy in xenografted human cancer using beta-camera and immunohistochemistry. *Aust NZ J Med* 1989.
18. Schrack RA. A microchannel plate neutron detector. *Nucl Instrum Methods Phys Res* 1984; 222:499-506.
19. Paresce F, Clampin M, Cox C, et al. The ranicon for ground-based optical astronomy. In: Robinson L., ed. *Space Telescope Science Institute preprint series no 225*. New York: Springer-Verlag; 1987.
20. Clampin M, Crocker J, Paresce F, Rafal M. Optical ranicon detectors for photon counting imaging. 1. *Rev Sci Instrum* 1988; 59:1269-1285.
21. Wanying Q, Persson E-C, Ingvar C, Norrgren K, Brodin T, Strand S-E. Comparative biokinetics of rat monoclonal IgM antibody radiolabeled with <sup>125</sup>I and internally with <sup>35</sup>S in rats bearing rat colon carcinoma. *Proceedings Fourth international conference on monoclonal antibody immunoconjugates for cancer*. 1989; 30:112.